A Theory Of Spherical Harmonic Identities for BRDF/Lighting Transfer and Image Consistency

Dhruv K. Mahajan

Submitted in fulfillment of the
requirements for the Masters Degree
in the Computer Science Department

COLUMBIA UNIVERSITY

2006

ABSTRACT

A Theory Of Spherical Harmonic Identities for BRDF/Lighting Transfer and Image Consistency

Dhruv K. Mahajan

We develop new mathematical results based on the spherical harmonic convolution framework for reflection from a curved surface. We derive novel identities, which are the angular frequency domain analogs to common spatial domain invariants such as reflectance ratios. They apply in a number of canonical cases, including single and multiple images of objects under the same and different lighting conditions. One important case we consider is two different glossy objects in two different lighting environments. Denote the spherical harmonic coefficients by $B_{lm}^{light,material}$ where the subscripts refer to the spherical harmonic indices, and the superscripts to the lighting (1 or 2) and object or material (again 1 or 2). We derive a basic identity, $B_{lm}^{1,1}B_{lm}^{2,2} = B_{lm}^{1,2}B_{lm}^{2,1}$, independent of the specific lighting configurations or BRDFs. While this paper is primarily theoretical, it has the potential to lay the mathematical foundations for two important practical applications. First, we can develop more general algorithms for inverse rendering problems, which can directly relight and change material properties by transferring the BRDF or lighting from another object or illumination. Second, we can check the consistency of an image, to detect tampering or image splicing. In summary, this thesis introduces the basic theory, that can lead to much future theoretical and practical work in inverse rendering and image consistency checking.

Acknowledgements

Firstly, I would like to thank my advisor, Prof. Ravi Ramamoorthi. Insightful discussions with him motivated me to pursue active research in computer vision and computer graphics as my career. It has been a wonderful experience for me to work with him during my thesis. I would also like to thank Prof. Brian Curless, with whom I had several long discussions during different stages of the thesis.

In the two years spent here, I have interacted with several people in the Columbia vision and graphics centre. I would particularly like to thank Kshitiz Garg for giving me valuable feedback during the project and having several long discussions with me regarding my career. I would also like to thank Sameer Agarwal for many helpful discussions.

This work was supported by NSF grant # 0430258 (CyberTrust - Restore the Trustworthiness of Digital Photographs: Blind Detection of Digital Photograph Tampering), as well as NSF grants # 0098005, # 0305322 and # 0446916, the Washington Research Foundation, Microsoft Research, and the University of Washington Animation Research Labs.

Contents

List of Figures

Chapter 1

Introduction

The study of the appearance of objects with complex material properties in complex lighting is one of the challenging problems in both computer vision and computer graphics. Variability in lighting has a huge effect on the appearance of objects in images. As a result, the recognition of objects like faces under unknown complex lighting conditions is an area of active interest in computer vision. Moreover, we need to model complex material properties and lighting to create realistic computer generated images. Therefore, inverse rendering methods are extensively used in computer graphics to measure these attributes from real photographs.

Substantial progress has been made in the analysis of Lambertian objects in complex lighting. Recent work by Basri and Jacobs [BJ03], and Ramamoorthi and Hanrahan [RH01b] has shown that the appearance of a curved surface can be described as a spherical convolution of the (distant) illumination and BRDF. They assume curved homogeneous objects (single BRDF) of known shape lit by complex distant illumination, and neglect cast shadows and interreflections. They prove that the set of all Lambertian reflectance functions (the mapping from surface normals to intensities) lies close to a 9D linear subspace. This result often enables computer vision algorithms, previously restricted to point sources without attached shadows, to work in general complex lighting and has led to a number of novel algorithms for lighting-insensitive recognition, photometeric stereo, and even fast rendering in computer graphics [BJ03, RH01a, BJ01, RH02, SKS02, HS05].

However, there has been relatively little work in vision on using the convolution formulae for glossy objects, even though the frequency analysis [RH01b] applies for general materials. The main goal of this thesis is to derive new formulae and identities for direct frequency domain spherical (de)convolution. Our work is based on the spherical convolution theory of Ramamoorthi and Hanrahan [RH01b]. In addition to assumptions made by them, we also assume that the BRDF is radially symmetric, which is a good approximation for most specular reflectance. Specifically, we make the following theoretical contributions:

Derivation of New Frequency Domain Identities: Our main contribution is the derivation of a number of new theoretical results, involving a class of novel frequency domain identities. We study a number of setups, including single (chapters 5 and 6) and multiple (chapter 7) images under single and multiple lighting conditions. For example, one important case we consider (section 7.3) is that of two different glossy[1] materials in two different lighting environments. Denote the spherical harmonic coefficients by $B_{lm}^{light,material}$, where the subscripts refer to the harmonic indices, and the superscripts to the lighting (1 or 2) and object or material (again 1 or 2). We derive an identity for the specular component, $B_{lm}^{1,1}B_{lm}^{2,2} = B_{lm}^{1,2}B_{lm}^{2,1}$, directly from the properties of convolution, *independent* of the specific lighting configurations or BRDFs.

Analogy between Spatial and Frequency Domain Invariants: By definition, invariants are insensitive to certain appearance parameters like lighting. They usually transform images to a simple feature space where more accurate algorithms can be developed for the task at hand (for example, lighting-insensitive recognition). We show (chapter 8) that the class of identities derived in the thesis can be considered the analog in the frequency domain of fundamental spatial domain invariants, such as reflectance ratios (Nayar and Bolle [NB96]) or photometric invariants (Narasimhan et al. [NRN03]). We consider curved homogeneous glossy objects instead of textured Lambertian objects. Also, we consider general complex lighting, while much of the previous spatial domain theory is limited to single

[1]Parts of the theory (in chapters 5 and 7) address only purely specular (or purely Lambertian) objects. However, as discussed in the thesis and shown in our results, the theory and algorithms can be adapted in practice to glossy objects having both diffuse and specular components. Hence, we use the term “glossy” somewhat loosely throughout the thesis.

point sources.

Analysis of Diffuse Irradiance in Reflected Parameterization: Another major contribution of the thesis is the analysis of diffuse irradiance in the reflected parameterization. This allows us to study objects with both diffuse and specular components in a unified framework. We show that even with the parameterization by reflected direction, the effects of diffuse irradiance are limited to low frequencies. To our knowledge, this is the first such combined diffuse plus specular theory and is likely to have broader implications for other problems in vision, such as photometric stereo and light-insensitive recognition.

The theory and novel identities presented in the thesis have potential applications in many areas of vision and graphics like inverse rendering, consistency checking, BRDF-invariant stereo and photometric stereo or lighting-insensitive recognition. In particular, this thesis is motivated by the following three important practical applications, and seeks to lay the mathematical foundations in these areas.

Inverse Rendering: Estimation of the BRDF and lighting has been an area of active research in vision and graphics. Inverse Rendering deals with measuring these rendering attributes from photographs. Rendering synthetic images by using these measurements from real objects greatly enhances the visual realism of the rendered images. For example, we estimate illumination from a single image of a glossy material with known BRDF. By the convolution theorem, a glossy material will reflect a blurred version of the lighting. It is appealing to sharpen or deconvolve this by dividing in the frequency domain by the spherical harmonic coefficients of the BRDF. The basic formula is known [RH01b], but cannot be robustly applied, since BRDF coefficients become small at high frequencies. Our contribution is the adaptation of Wiener filtering [GW03, Wie42] from image processing to develop robust deconvolution filters (figures 4.3 and 9.2). We are able to amplify low frequencies to recover the lighting and reduce noise simultaneously.

BRDF/Lighting Transfer: Besides estimation of lighting and BRDFs, we also develop more general algorithms, which directly relight and change material properties by transferring the BRDF or lighting from another object or illumination. For example, we

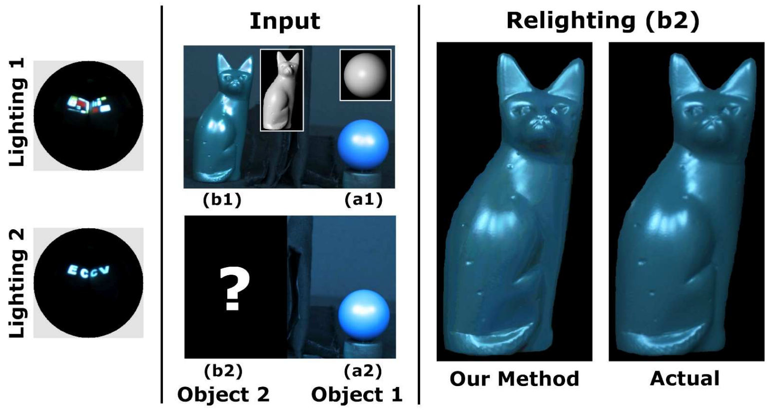

Figure 1.1: One application of our framework. We are given real photographs of two objects of known geometry (shown in inset; note that both objects can be arbitrary, and one of them is a sphere here only for convenience). The two objects have different (and unknown) diffuse and specular material properties. Both objects are present in the first image under complex lighting, but the cat is not available in the second image, under new lighting. *Unlike previous methods, none of the lighting conditions or BRDFs are known* (lightings on left shown only for reference). Our method enables us to render or relight the cat, to obtain its image in lighting 2 (compare to actual shown on the right). This could be used for example to synthetically insert the cat in the second image.

derive the identity $B^{1,1}_{lm}B^{2,2}_{lm} = B^{1,2}_{lm}B^{2,1}_{lm}$, where $B^{i,j}$ denote the image of object j in lighting i. This identity enables us to render the fourth light/BRDF image (say $B^{2,2}_{lm}$), given the other three, *without explicitly estimating any lighting conditions or BRDFs.* A common example (figure 1.1) is when we observe two objects in one lighting, and want to insert the second object in an image of the first object alone under new lighting. It is difficult to apply conventional inverse rendering methods in this case, since none of the illuminations or BRDFs are known.

Image Consistency Checking and Tampering Detection: The final, newer application, is to verify image consistency and detect tampering (Johnson and Farid [JF05], Lin et al. [LWTS05]). The widespread availability of image processing tools enables users to create "forgeries" such as by splicing images together (one example is shown in figure 9.3).

Moreover, watermarking is not usually a viable option in many applications, such as verifying authenticity for news reporting. However, (in)consistencies of lighting, shading and reflectance can also provide valuable clues. This thesis takes an important first step in laying the theoretical foundations for this new research direction, by deriving a new class of identities which can be checked to ensure image consistency.

The next chapter discusses the previous work done in related areas. We briefly explain the spherical convolution and signal processing framework in chapter 3. Chapter 4 demonstrates the use of deconvolution to estimate lighting. In chapters 5 and 6, we introduce identities for the simple case of a single image of an object. Chapter 7 derives more identities for the case of multiple images. In chapter 8 we discuss the implications of our theory and its relation with spatial domain invariants. Chapter 9 gives experimental validation of our theory and shows potential applications. Finally, we conclude our discussion in chapter 10 and talk about the future research directions that this work makes possible. This thesis is an extended and detailed version of the work [MRC06] to be presented at ECCV2006.

Chapter 2

Previous Work

The theory discussed in the thesis has implications to a broad range of areas in vision and graphics. This chapter briefly touches upon the related work in these areas.

Spherical Harmonics and Convolution Theorem: As discussed in the introduction, our work is derived from the spherical convolution theory of Basri and Jacobs [BJ03], and Ramamoorthi and Hanrahan [RH01b]. They show that the appearance of a curved surface can be described as a spherical convolution of the (distant) illumination and BRDF and hence as their product in the spherical harmonics or frequency domain. Many recent articles in computer vision have explored theoretical and practical applications for Lambertian surfaces (e.g., [BJ01, SFB03]). In graphics, the general convolution formulae have been used for rendering with environment maps [RH02], and insights have been widely adopted for forward and inverse rendering (e.g., [RH01b, SKS02]). However, as noted earlier, direct application of the convolution theorem for general materials is still rare.

Image Relighting and Inverse Rendering: Given images of an object under a sparse set of lighting condition(s), relighting it with novel lighting is an interesting problem. Current methods [MWLT00, MG97, SSI99] require explicit estimation of lighting and BRDF from the images of a scene. This thesis presents a novel identity to directly relight and change material properties without explicit estimation of BRDF or illumination.

Spatial Domain Invariants: As discussed above, the direct estimation of parameters like lighting and BRDF from a set of images of a scene is a hard problem. Invariants provide an intermediate solution to this problem. They have been previously used mostly for material and lighting insensitive recognition [NRN03, DYW05]. There has been a lot of previous work in developing spatial domain invariants. Nayar and Bolle [NB96] compute the ratio of intensities at adjacent pixels to derive lighting independent reflectance ratios. Davis et al. [DYW05] derive a similar BRDF independent ratio. Narsimhan et al. [NRN03] consider a summation of multiple terms (diffuse plus specular), where each term is a product of lighting, BRDF and scene geometry. However most of the above methods are limited to point sources [NRN03, DYW05] and consider textured Lambertian objects only [DYW05, NB96].

We for the first time derive the frequency domain analogs to these common spatial domain invariants. Our frequency domain identities have a simple form and generalize well to complex lighting and object materials. However we assume curved homegeneous objects of known geometry. Moreover while our identities operate globally needing the full range of reflected directions, spatial domain invariants involve mostly local pixel-based operations.

Image Consistency Checking and Tampering Detection: This is a new interesting area of research. (In)Consistency in shading can provide important clues for tampering detection. Most previous work has focused on checking consistency at a signal or pixel level, such as the camera response [LWTS05], or wavelet coefficients (Ng et al. [NCS04]). But most of these methods do not exploit consistencies of lighting, shading and reflectance. Johnson and Farid [JF05] detect inconsistencies in lighting to expose forgeries. But their method is limited to point light sources. Our frequency domain identities can be used directly to detect tampering and consistency of lighting and shading in a complex lighting environment.

Chapter 3

Background

We now briefly introduce the spherical convolution and signal-processing framework [BJ03, RH01b] needed for our later derivations. We start with the Lambertian case,

$$B(\mathbf{n}) = \int_{S^2} L(\omega) \max(\mathbf{n} \cdot \omega, 0) \, d\omega, \tag{3.1}$$

where $B(\mathbf{n})$ denotes the reflected light as a function of the surface normal. B is proportional to the irradiance (we omit the albedo for simplicity), and $L(\omega)$ is the incident illumination. The integral is over the sphere S^2, and the second term in the integrand is the *half-cosine* function. The equations in this paper do not explicitly consider color; the (R,G,B) channels are simply computed independently. A similar mathematical form holds for other radially symmetric BRDFs, such as the Phong model for specular materials. In this case, we reparameterize by the reflected direction $\mathbf{R}$ (the reflection of the viewing ray about the surface normal), which takes the place of the surface normal:

$$B(\mathbf{R}) = \frac{s+1}{2\pi} \int_{S^2} L(\omega) \max(\mathbf{R} \cdot \omega, 0)^s \, d\omega, \tag{3.2}$$

where s is the Phong exponent, and the BRDF is normalized (by $(s+1)/2\pi$).

If we expand in spherical harmonics $Y_{lm}(\theta, \phi)$, using spherical coordinates $\omega = (\theta, \phi)$, $\mathbf{n}$ or $\mathbf{R} = (\alpha, \beta)$, and $\rho(\theta)$ for the (radially symmetric) BRDF kernel, we obtain

$$L(\theta, \phi) = \sum_{l=0}^{\infty} \sum_{m=-l}^{l} L_{lm} Y_{lm}(\theta, \phi) \qquad B(\alpha, \beta) = \sum_{l=0}^{\infty} \sum_{m=-l}^{l} B_{lm} Y_{lm}(\alpha, \beta) \qquad \rho(\theta) = \sum_{l=0}^{\infty} \rho_l Y_{l0}(\theta). \tag{3.3}$$

It is also possible to derive analytic forms and good approximations for common BRDF filters ρ. For the Lambertian case, almost all of the energy is captured by $l \leq 2$. For

Phong and Torrance-Sparrow, good approximations [RH01b] are Gaussians: $\exp[-l^2/2s]$ for Phong, and $\exp[-(\sigma l)^2]$ for Torrance-Sparrow, where σ is the surface roughness parameter in the Torrance-Sparrow model, and s is the Phong exponent.

In the frequency domain, the reflected light B is given by a simple product formula or spherical convolution (see [BJ03, RH01b] for the derivation and an analysis of convolution),

$$\boxed{B_{lm} = \Lambda_l \rho_l L_{lm} = A_l L_{lm},} \tag{3.4}$$

where for convenience, we define the normalization constant Λ_l as

$$\Lambda_l = \sqrt{\frac{4\pi}{2l+1}} \qquad A_l = \Lambda_l \rho_l. \tag{3.5}$$

It is also possible to extend these results to non-radially symmetric general isotropic BRDFs [RH01b]. For this case, we must consider the entire 4D light field, expressed as a function of both orientation and outgoing direction,

$$B_{lmpq} = \Lambda_l \rho_{lq,pq} L_{lm}, \tag{3.6}$$

where the reflected light field is now expanded in a mixed basis of representation matrices and spherical harmonics, and has four indices because it is a 4D quantity. The 3D isotropic BRDF involves an expansion over both incoming and outgoing directions.

The remainder of this thesis derives new identities and formulae from equation 3.4, $B_{lm} = A_l L_{lm}$. We focus on equation 3.4, since it is simple, and allows practical spherical harmonic computations from only a *single image*—a single view of a sufficiently curved object (assuming a distant viewer) sees all reflected directions[1]. Most glossy BRDFs (such as Torrance-Sparrow) are approximately radially symmetric, especially for non-grazing angles of reflection [RH01b, RH02]. Most of the theory in this thesis also carries over to general isotropic materials, as per equation 3.6, if we consider the entire light field.

---

[1]In case we do not have the full range of normals, we can use multiple cameras. As we move the camera(viewer) the same point on the object now corresponds to a different reflected direction. Hence we can get all the reflected directions even if the object has only a partial set of normals by the careful placement of cameras.

Chapter 4

Known BRDF: Deconvolution to Estimate Lighting

Lighting Estimation is a specific example of the general inverse rendering problem. Given a single image and BRDF of an object, we want to estimate the directional distribution of the incident light. This information can then be used to insert new objects in the scene, alter the lighting of the object or check lighting consistency between two objects. Since reflected light (image) is a spherical convolution of lighting and BRDF, it makes sense to deconvolve it to estimate lighting. We present a deconvolution algorithm for curved surfaces under complex lighting. Section 4.1 describes the basic deconvolution idea and introduces an ideal deconvolution filter. We then discuss the properties of this filter for Phong-like BRDFs in section 4.2. Section 4.3 describes the Wiener regularization used to regularize the inverse filter so that it can be used for practical purposes. Finally, we show the results of applying this filter in section 4.4.

4.1 Deconvolution - Basic Idea

Given a single image of a curved surface, we can map local viewing directions to the reflected direction, determining $B(\mathbf{R})$, and then B_{lm} by taking a spherical harmonic transform. If the material includes a diffuse component as well as specular, we use the dual lighting estimation algorithm of Ramamoorthi and Hanrahan [RH01b], which estimates the specular B_{lm} consistent with the diffuse component. As per equation 3.4, B_{lm} will be a blurred version of the original lighting, filtered by the glossy BRDF.

From equation 3.4 in the spherical harmonic domain, we derive

$$L_{lm} = \frac{B_{lm}}{A_l} = {A_l}^{-1} B_{lm}, \tag{4.1}$$

where the last identity makes explicit that we are convolving with a new radially symmetric kernel A_l^{-1}, which can be called the inverse, sharpening or deconvolution filter. A_l^{-1} effectively amplifies high frequencies to recover blurred out details.

4.2 Analysis of Inverse Phong Filter

We now discuss the properties of the angular form of the inverse filter. Surprisingly, not much work has been done to analyze this filter in detail. For simplicity, we will use the Fourier transform rather than spherical harmonics. We will illustrate that the properties discussed in the Fourier domain are also valid for spherical harmonics.

We use inverse Phong filter for our analysis. As mentioned earlier, Gaussian $\exp[-l^2/2s]$ gives a good approximation for Phong, where s is the Phong exponent. So, the inverse Phong filter can be approximated by $\exp[l^2/2s]$. For applying this filter practically, we need to truncate it first to a cutoff frequency m. The inverse Fourier transform of this truncated filter is

$$f(x, m, s) = \int_{-m}^{m} e^{\frac{u^2}{2s}} e^{2\pi i x u} du \tag{4.2}$$

Putting $u = \sqrt{2s}v$

$$f(x, m, s) = \sqrt{2s} \int_{-\frac{m}{\sqrt{2s}}}^{\frac{m}{\sqrt{2s}}} e^{v^2} e^{2\sqrt{2s}\pi i v x} dv$$

$$\begin{aligned} f(x, m, s) &= \sqrt{2s} g(\sqrt{2s}x, \frac{m}{\sqrt{2s}}), && (4.3) \\ g(x, k) &= \int_{-k}^{k} e^{t^2} e^{2\pi i t x} dt && (4.4) \end{aligned}$$

$g(x, k)$ is the inverse Fourier transform of the cannonical filter $\exp[t^2]$ truncated at k and is independent of Phong exponent s. Going from f to g is just the application of Fourier Scale Theorem. Let $H(u)$ be the Fourier transform of $h(x)$.

$$h(x) \leftrightarrow H(u)$$

Then, the Fourier scale theorem says that

$$h(ax) \leftrightarrow \frac{1}{|a|} H(\frac{u}{a})$$

In our case $a = \frac{1}{\sqrt{2s}}$. The frequencies u of the cannonical filter $\exp[u^2]$ get scaled by $\frac{1}{\sqrt{2s}}$. By the Fourier scale theorem, this means that x gets scaled by $\sqrt{2s}$ in the spatial domain. Hence $f(x, m, s)$ is just the spatially scaled version of $g(x, k)$. $g(x, k)$ can be further simplified as

$$g(x,k) = \frac{2\pi e^{k^2}}{k} n(kx, \frac{\pi}{k}), \tag{4.5}$$

$$n(\alpha, \beta) = \int_{\alpha}^{\infty} e^{\beta^2(\alpha^2 - u^2)} sin(2\pi u) du \tag{4.6}$$

A detailed derivation is given in Appendix A. $n(\alpha, \beta)$ can be considered as a normalized form of the inverse filter and is independent of both Phong exponent s and cutoff frequency m. Plots for $f(x, m, s), g(x, k)$ and $n(\alpha, \beta)$ are shown in figure 4.1(a)-(f). Here k and m are related to each other by $k = \frac{m}{\sqrt{2s}}$. We now discuss some important properties of $f(x, m, s)$.

4.2.1 Periodicity:

We have found empirically that $n(\alpha, \beta)$ has a period 1 in α (figure 4.1(c,f)). Hence $g(x, k)$ has period $\frac{1}{k}$ (from equation 4.5). From equation 4.3,

$$\begin{aligned} \text{Period of } f(x,m,s) &= \frac{1}{\sqrt{2s}} * \text{Period of } g(x,k) \\ &= \frac{1}{\sqrt{2s}} * \frac{1}{k} \\ &= \frac{1}{\sqrt{2s}} * \frac{\sqrt{2s}}{m} \\ &= \frac{1}{m} \end{aligned} \tag{4.7}$$

So as cutoff frequency m increases, filter becomes more and more oscillatory (figure 4.1(a,d)).

4.2.2 Amplitude:

We now discuss the effect of truncation m and Phong exponent s on the amplitude of the filter f(at $x = 0$). The next subsection discusses the amplitude fall-off of the filter.

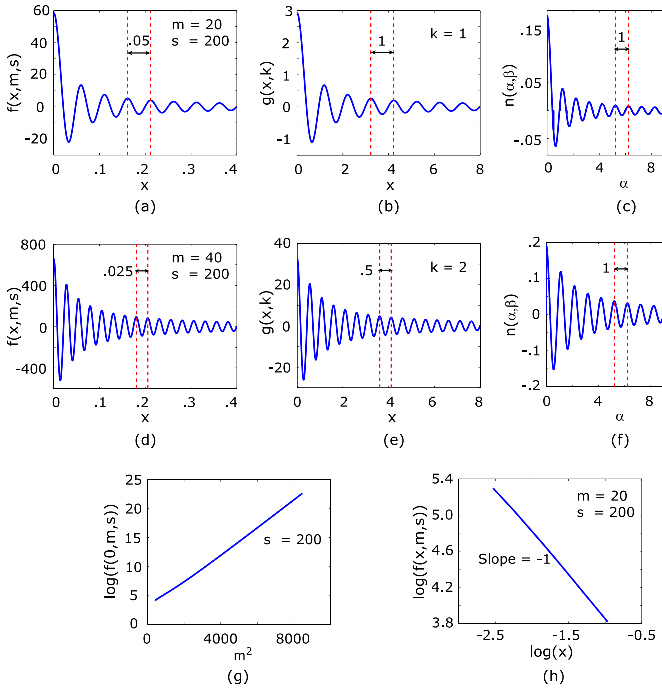

Figure 4.1: **Row 1 and 2:** f, g and n functions for two different values of frequency cut-off m. As m increases, f become more and more oscillatory with period $\frac{1}{m}$. The period of n however does not change. **Bottom Row:** (g) shows that the amplitude of f (at $x = 0$) increases exponentially with m^2. The log-log plot (h) of amplitude of f vs. x is a straight line with slope -1, showing that filter falls off as $\frac{1}{x}$.

Equations 4.3 and 4.5 suggest that amplitude introduced due to frequency cutoff m and Phong exponent s is

$$\sqrt{2s}\frac{e^{k^2}}{k} = \frac{2se^{\frac{m^2}{2s}}}{m} \tag{4.8}$$

As m increases, amplitude grows almost exponentially, as can be seen from figure 4.1(g)

4.2.3 Amplitude Fall-off:

Amplitude fall-off of $f(x, m, s)$ is same as that of $n(\alpha, \beta)$. Figure 4.1(h) shows that the log-log plot of amplitude falloff for $f(x, m, s)$ is a straight line with *slope* $= -1$. *Hence amplitude of $f(x, m, s)$ falls off as* $\frac{1}{x}$ with x.

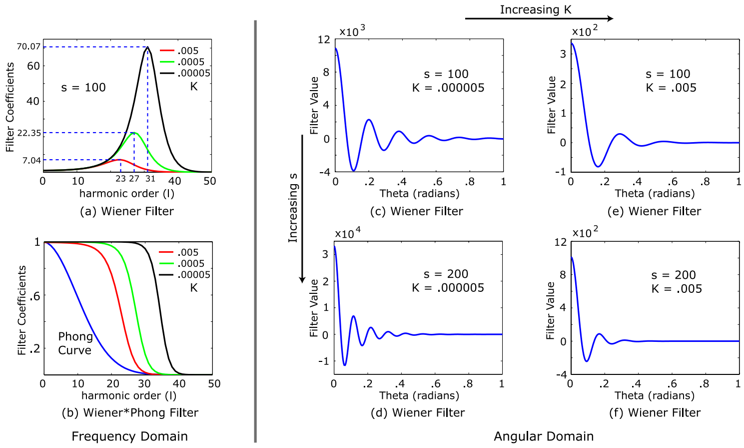

Figure 4.2: **Left:** Wiener filters in frequency domain. (a) shows the Wiener filters for different values of K for Phong BRDF ($s = 100$). Note that the maxima occurs at $l^* = \sqrt{log(\frac{1}{K^s})}$, the value being $A_l^{*max} = \frac{1}{2\sqrt{K}}$. The convolution of the filter (a) with the original Phong filter (blue graph in b) lets through most frequencies without attenuation, while filtering out the very high frequencies. **Right:** Wiener filters in angular domain. Note the decrease in oscillations as we increase the value of K (c,e and d,f). Also the period of the filter decreases with increasing Phong exponent s (c,d and e,f).

4.3 Wiener Regularization

Section 4.2 shows that it is difficult to apply equation 4.1 directly and we need regularization. However a hard cutoff at a certain frequency is not best to reduce ringing or for practical implementation.

These types of problems have been well studied in image processing, where a number of methods for deconvolution have been proposed. We adapt Wiener filtering [GW03, Wie42] for this purpose. Specifically, we define a new inverse filter,

$$A_l^* = \frac{1}{A_l}\left(\frac{\mid A_l \mid^2}{\mid A_l \mid^2 + K}\right) = \frac{A_l}{\mid A_l \mid^2 + K} \qquad\qquad L_{lm} = A_l{}^* B_{lm}, \tag{4.9}$$

where K is a small user-controlled constant. When $\mid A_l \mid^2 \gg K$, the expression in parentheses on the left is close to 1, and $A_l^* \approx A_l^{-1}$. When $\mid A_l \mid^2 \ll K$, $A_l^* \approx A_l/K$.

Figure 4.2 shows the Wiener filter in spatial and frequency domain for Phong BRDF with different Phong exponents and K values. Note the smooth falloff of the filter in the frequency

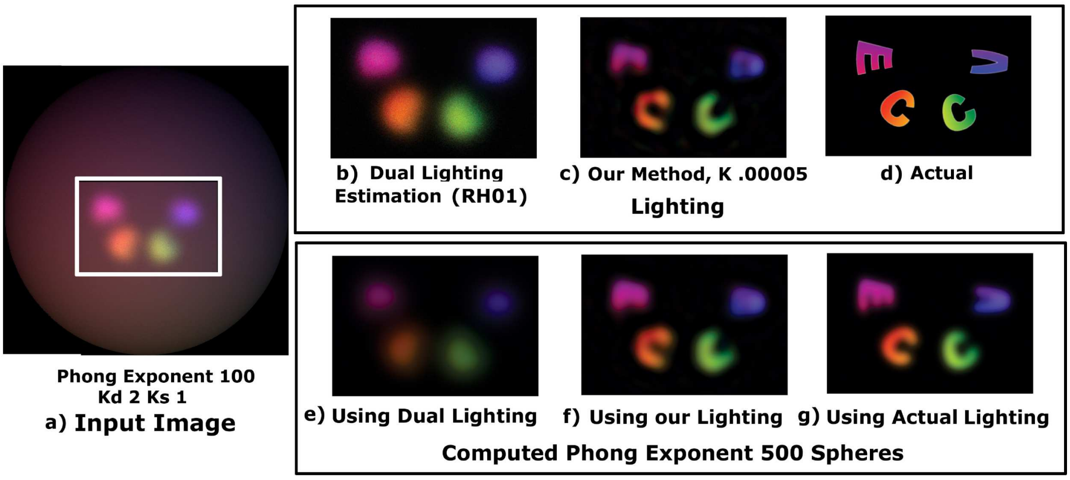

Figure 4.3: **(a):** Original synthetic image (Phong BRDF with exponent $s = 100$, diffuse $K_d = 2$ and specular $K_s = 1$) with noise—close examination of (a),(b) will reveal the noise. **Top row:** We recover (c) the "ECCV" text in the original lighting (d). Previous techniques (b) can estimate only a blurred result. Note that top and bottom rows show a closeup of the sphere. **Bottom row:** We can use the recovered illumination to create a new rendering of a high-frequency material (f). This compares well with the actual result (g); a previous method (e) creates a very blurred image.

domain.. The maxima obtained by differentiating equation 4.9 occurs at $A_l^{max} = \sqrt{K}$ with the maximum value $A_l^{*max} = \frac{1}{2\sqrt{K}}$. A_l^{max} can be thought of as the effective cutoff frequency value of the filter. For Phong filter $\exp[-l^2/2s]$, this corresponds to the cutoff frequency $l^* = \sqrt{log(\frac{1}{K^s})}$. For a given s, as K increases, l^* decreases and hence more and more of the higher frequencies get truncated. The convolution of the filter (a) with the original Phong filter (blue graph in b) lets through most frequencies without attenuation, while filtering out the very high frequencies. (c)-(f) shows these filters in the angular domain. Inreasing the value of K(c,e and d,f) decreases the amplitude of the filter and makes it less oscillatory, thus decreasing the ringing effects. Increasing the Phong exponent s(c,d and e,f) decreases the periodicity of the filter.

4.4 Lighting Estimation in Frequency Domain

The top row in figure 4.3 shows the results (on the synthetic noisy sphere in (a)) of deconvolution (c)—the “ECCV” text used in the lighting (d) can be recovered fairly clearly. One interesting point is the effect of noise. In our case, the image in a glossy surface is already low pass filtered (because of the BRDF), while any noise usually has much higher frequency content, as seen in the original synthetic image (a). The filter in equation 4.9 amplifies the low frequencies (to invert the effects of low-pass filtering), but reduces the high frequencies (because of the inherent regularization). Hence, we can *simultaneously deconvolve the lighting and suppress noise* (compare the noise in (c) with that in (a) or (b)). Figure 9.2 shows an application of our method with real data and a geometrically complex object.

It is also interesting to compare our results to previous techniques. Angular-domain approaches are usually specialized to point lights, use higher-frequency information like shadows (Sato et al. [SSI99]) or recover large low-frequency lighting distributions (Marschner and Greenberg [MG97]). Even the more precise dual angular-frequency lighting estimation technique of Ramamoorthi and Hanrahan [RH01b] can obtain only a blurred estimate of the lighting (b). The effect of these results is clearly seen in the bottom row of figure 4.3, where [RH01b] produces a blurred image (e) when trying to synthesize renderings of a new high-frequency material, while we obtain a much sharper result (f).

Chapter 5

Theoretical Analysis: Single Image of one Object with specular BRDF

We now carry out our theoretical analysis and derive a number of novel identities for image consistency checking and relighting. We structure the discussion from the simplest case of a single image of one object in this section, to more complex examples in chapter 7—two objects in the same lighting, the same object in two lighting conditions, and finally two (or many) objects in two (or many) lighting conditions. Deconvolution discussed in chapter 4 is a special single image case where we know the BRDF of the object but lighting is unknown. In this section we discuss the converse case, where the lighting is known, but the BRDF is unknown. The objects are assumed to be purely specular. We then present a general theory for objects with both diffuse and specular components in the next section.

We show that for radially symmetric specular BRDFs, described using equation 3.4, we can *eliminate* the BRDF to derive an identity that must hold and can be checked *independent of the BRDF*. This is the first of a number of frequency domain identities we will derive in a similar fashion. First, from equation 3.4, we can write

$$A_l = \frac{B_{lm}}{L_{lm}}. \tag{5.1}$$

This expression could be used to solve for BRDF coefficients[1]. However, we will use it in a

[1]Since natural lighting usually includes higher frequencies than the BRDF, we can apply equation 5.1 directly without regularization, and do not need to explicitly discuss deconvolution—however, the next

different way. Our key insight is that the above expression is independent of m, and must hold for all m. Hence, we can eliminate the (unknown) BRDF A_l, writing

$$\frac{B_{li}}{L_{li}} = \frac{B_{lj}}{L_{lj}} \tag{5.2}$$

for all i and j. Moving terms, we obtain our first identity,

$$B_{li}L_{lj} - B_{lj}L_{li} = 0. \tag{5.3}$$

For checking the consistency of images, the above identity can be used without needing to explicitly know or calculate the BRDF. In effect, we have found a redundancy in the structure of the image, that can be used to detect image tampering or splicing. To normalize identities in a [0...1] range, we always use an error of the form

$$\text{Error} = \frac{\mid B_{li}L_{lj} - B_{lj}L_{li} \mid}{\mid B_{li}L_{lj} \mid + \mid B_{lj}L_{li} \mid}.$$

There are many ways one could turn this error metric into a binary consistency checker or tamper detector. Instead of arbitrarily defining one particular approach, we will show graphs of the average normalized error for each spherical harmonic order.

Figure 5.1 applies our theory to synthetic data of an ideal Phong BRDF, with noise added. We show closeups of spheres generated with "ECCV" and "ICCV" lighting. To the naked eye, these look very similar, and it is not easy to determine if a given image is consistent with the lighting. However, our identity in equation 5.3 clearly distinguishes between consistent (i.e., the image is consistent with the lighting [ECCV or ICCV] it is supposed to be rendered with) and inconsistent illumination/image pairs. As compared to Johnson and Farid [JF05], we handle general complex illumination. Moreover, many of the identities in later sections work directly with image attributes, not even requiring explicit estimation or knowledge of the illumination.

Our framework could be used to blindly (without watermarking) detect tampering of images, making sure a given photograph (containing a homogeneous object of known shape)

chapter does derive a new robust formula (equation 6.4) for BRDF estimation when *both* diffuse and specular components are present. Conversely, the frequency space identity in this chapter (equation 5.3) cannot be derived for the known BRDF case, since the lighting is not radially symmetric and therefore cannot be eliminated.

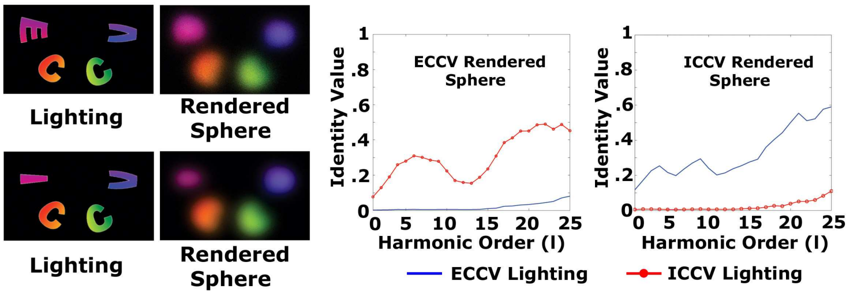

Figure 5.1: **Left:** The synthetic images used. These correspond to closeups of specular spheres rendered with "ECCV" and "ICCV" lighting. To the naked eye, the two images look very similar. **Middle and Right:** The graphs show that our identity can clearly distinguish consistent image/lighting pairs (lower line) from those where lighting and image are inconsistent (upper line).

is consistent with the illumination it is captured in.[2] To the best of our knowledge, ours is the first theoretical framework to enable these kinds of consistency checks. Example applications of tamper detection on real objects are shown in figures 9.1 and 9.3.

Finally, it should be noted that if we are given the full light field (all views) instead of simply a single image, a similar identity to equation 5.3 holds for general BRDFs that need not be radially symmetric. In particular, from equation 3.6,

$$B_{lipq}L_{lj} - B_{ljpq}L_{li} = 0. \tag{5.4}$$

For the rest of this thesis, we will not explicitly write out the form of the identities for general light fields, but it should be understood that similar properties can be derived for general isotropic BRDFs and light fields for most of the formulae we discuss here.

[2] Our identities are "necessary" conditions for image consistency, under our assumptions and in the absence of noise. They are not theoretically "sufficient". For example, if an unusual material were to zero out a certain frequency, tampering at that frequency may go undetected. Also note that noise tends to add high frequencies, while materials tend to filter out high frequencies, causing the consistency errors to rise (become less reliable) with harmonic order.

Chapter 6

Single Image: Combining Diffuse and Specular

We now consider the more general case of an unknown glossy BRDF with both specular *and* Lambertian (diffuse) reflectance. To our knowledge, this is the first such combined diffuse plus specular theory of the single image case, and the analysis (such as equations 6.1 and 6.4) is likely to have broader implications for other problems in vision, such as photometric stereo and lighting-insensitive recognition. Some readers may wish to skim this chapter, which is slightly more technical, on a first reading of the thesis.

6.1 Common Parameterization

The major technical difficulty is that while both diffuse (Lambertian) and specular components are radially symmetric, they are so in different parameterizations (normal vs reflected direction). An important technical contribution of this thesis is to express the diffuse irradiance in the reflected parameterization,

$$B_{lm} = K_d D_{lm} + A_l^{\mathrm{spec}} L_{lm}. \tag{6.1}$$

The parameters of reflectance are the diffuse coefficient K_d and the specular BRDF filter coefficients A_l (we drop the superscript from now on). D_{lm} are the spherical harmonic coefficients of the irradiance written in the reflected parameterization. They depend linearly on the lighting coefficients L_{lm} (assumed known) as $D_{lm} \approx \sum_{n=0}^{2} A_n^{\mathrm{Lamb}} L_{nm} T_{lmn}$,

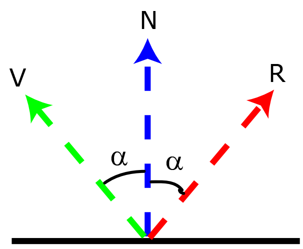

Figure 6.1: Reflected vs Normal Parameterization

with $T_{lmn} = \int_{S^2} Y_{nm}(\frac{\alpha}{2}, \beta) Y^*_{lm}(\alpha, \beta)\, d\Omega$. The $\alpha/2$ in the first term converts from normal to reflected parameterization. Figure 6.1 shows the relation between reflected and normal parameterization. Assuming that the coordinate system is aligned with the viewing direction $\mathbf{V}$, if normal $\mathbf{N}$ makes an angle α with $\mathbf{V}$, the reflected direction $\mathbf{R}$ makes an angle 2α. [1]

The coefficients T_{lmn} can be determined analytically or numerically, since the formulae for Y_{nm} and Y^*_{lm} are well known. Plots for D_{lm} and T_{lmn} are shown in figure 6.2 for a particular complex natural lighting environment. Since n ranges from 0 to 2 for Lambertian reflectance, m varies from -2 to $+2$, so we can safely neglect terms with $\mid m \mid > 2$ or $\mid n \mid > 2$. Moreover, for $l \geq 2$, we find that T_{lmn} either vanishes or falls off rapidly as $l^{-3/2}$ or $l^{-5/2}$. Hence, though somewhat more complex, Lambertian effects in the reflected parameterization are still relatively simple and low frequency. Please see Appendix B for a more detailed derivation.

6.2 Determining K_d and Image Consistency:

We now seek to eliminate A_l from equation 6.1 to directly estimate K_d for inverse rendering and reflectance estimation.

As before, A_l can be eliminated by considering different values of m,

$$\frac{B_{li} - K_d D_{li}}{L_{li}} = \frac{B_{lj} - K_d D_{lj}}{L_{lj}} \qquad \Longrightarrow \qquad K_d = \frac{B_{li} L_{lj} - B_{lj} L_{li}}{D_{li} L_{lj} - D_{lj} L_{li}}. \tag{6.2}$$

Since the above equation is true for all l,i,j, we also get an identity that must hold for

[1]We would like to emphasize that the reflected parameterization is not directly related to Rusinkiewicz's half-angle [Rus98]. In fact convolution theorem does not hold for the half-angle parameterization.

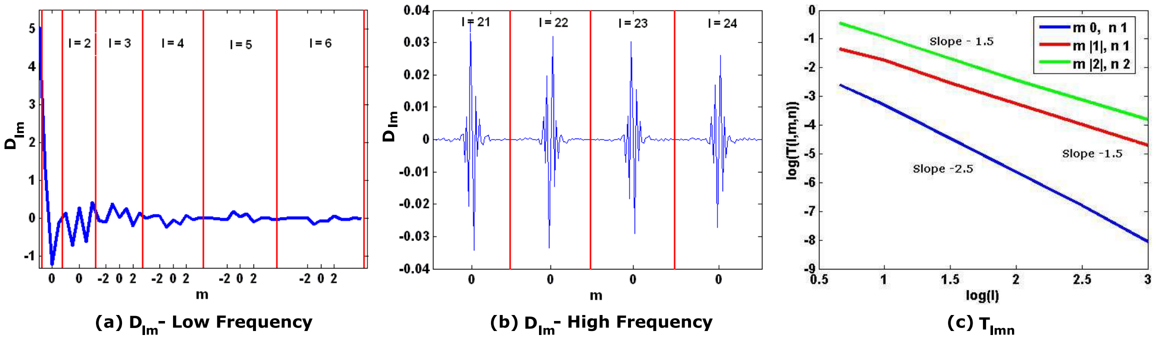

Figure 6.2: **(a),(b):** D_{lm} plots for low and high frequencies. Note that D_{lm} coefficients are neglegible for $\mid m \mid > 2$ and hence can be safely neglected. **(c):** T_{lmn} plot. T_{lmn} falls off rapidly as $l^{-3/2}$ or $l^{-5/2}$ for $l \geq 2$.

any l, i and j, and can be used for image consistency checking,

$$\frac{B_{l_1 i}L_{l_1 j} - B_{l_1 j}L_{l_1 i}}{D_{l_1 i}L_{l_1 j} - D_{l_1 j}L_{l_1 i}} = \frac{B_{l_2 m}L_{l_2 n} - B_{l_2 n}L_{l_2 m}}{D_{l_2 m}L_{l_2 n} - D_{l_2 n}L_{l_2 m}}. \tag{6.3}$$

6.3 Determining A_l and Image Consistency:

Equivalently, we can eliminate K_d,

$$\frac{B_{li} - A_l L_{li}}{D_{li}} = \frac{B_{lj} - A_l L_{lj}}{D_{lj}} \qquad \Longrightarrow \qquad A_l = \frac{B_{li}D_{lj} - B_{lj}D_{li}}{L_{li}D_{lj} - L_{lj}D_{li}}. \tag{6.4}$$

This can be used to directly estimate the specular BRDF coefficients, irrespective of the diffuse coefficient K_d. As a sanity check, consider the case when $K_d = 0$. In this case, $B_{li} = A_l L_{li}$, so the expression above clearly reduces to A_l. Hence, equation 6.4 can be considered a new robust form of reflectance estimation that works for both purely specular and general glossy materials. Further note that we estimate an accurate *non-parametric* BRDF representation specified by general filter coefficients A_l.

Since the formula above is true for all i, j, we get an identity for image consistency,

$$\frac{B_{li}D_{lj} - B_{lj}D_{li}}{L_{li}D_{lj} - L_{lj}D_{li}} = \frac{B_{lm}D_{ln} - B_{ln}D_{lm}}{L_{lm}D_{ln} - L_{ln}D_{lm}}. \tag{6.5}$$

Figure 6.3 shows these ideas applied to a synthetic sphere with both diffuse and specular components. In this case, we used as input A_l from measurements of a real material,

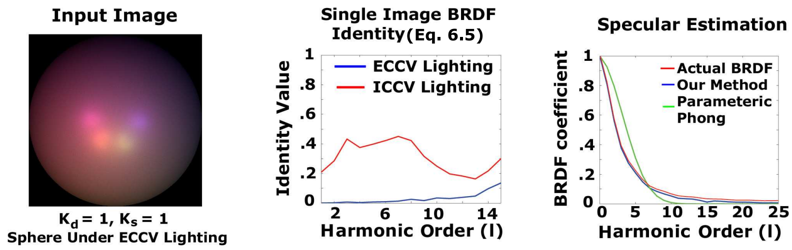

Figure 6.3: **Left:** Synthetic sphere image with both diffuse (K_d set to 1) and specular (taken from measurements of a real material) components. **Middle:** Image consistency checks (equation 6.5) can distinguish small inconsistencies between illumination and image ("ECCV" vs "ICCV" lighting). **Right:** For estimation of A_l, our approach gives accurate results, outperforming a parametric estimation technique.

and they *do not* correspond exactly to a Phong BRDF. Hence, our technique recovers the specular BRDF somewhat more accurately than a comparison method that simply does nonlinear estimation of Phong parameters. We also show image consistency checks similar to those in the previous section, using equation 6.5. As in the previous chapter, we can distinguish small inconsistencies between lighting and image. An application to detect splicing for a real object is shown in the left graph of figure 9.3.

Chapter 7

Theoretical Analysis: Two Materials and/or Lighting Conditions

Chapter 5 analyzed the single object, single image case. In this chapter[1], we first consider two different objects (with different materials) in the same lighting. Next, we consider one object imaged in two different lighting conditions. Then, we consider the two lighting/two BRDF case corresponding to two images (in different lighting conditions), each of two objects with distinct BRDFs. In the next chapter, we will discuss some broader implications.

7.1 Two Objects/BRDFs: Same Lighting

We consider a single image (hence in the same lighting environment) of two objects, with different BRDFs. Let us denote by superscripts 1 or 2 the two objects,

$$B^1_{lm} = A^1_l L_{lm} \qquad B^2_{lm} = A^2_l L_{lm}. \tag{7.1}$$

[1]This chapter will primarily discuss the purely specular case. For consistency checking, we have seen that in the reflective reparameterization, the diffuse component mainly affects frequencies D_{lm} with $\mid m \mid \leq 2$. Therefore, it is simple to check the identities for $\mid m \mid > 2$. Diffuse relighting is actually done in the spatial domain, as discussed in chapter 8. Chapter 9 provides experimental validation with objects containing both diffuse and specular components.

From these, it is possible to eliminate the lighting by dividing,

$$\frac{B_{lm}^2}{B_{lm}^1} = \frac{A_l^2}{A_l^1} = \gamma_l. \tag{7.2}$$

We refer to γ_l as the *BRDF transfer function.* Given the appearance of one object in complex lighting, multiplication of spherical harmonic coefficients by this function gives the appearance of an object with a different material. γ_l is *independent* of the lighting condition, and can be used in any (unknown) natural illumination. Also note that this function is *independent of* m, so we can average over all m, which makes it very robust to noise—in our experiments, we have not needed any explicit regularization for the frequencies of interest. Moreover, we do not need to know or estimate the individual BRDFs. It is not clear that one can derive such a simple formula, or bypass explicit lighting/reflectance estimation, in the spatial/angular domain. Section 7.3 will explore applications to rendering.

It is also possible to use these results to derive a frequency space identity that *depends only on the final images, and does not require explicit knowledge of either the lighting condition or the BRDFs.* We know that equation 7.2 should hold for all m, so

$$\frac{B_{li}^2}{B_{li}^1} = \frac{B_{lj}^2}{B_{lj}^1} \qquad \Longrightarrow \qquad B_{li}^2 B_{lj}^1 - B_{li}^1 B_{lj}^2 = 0. \tag{7.3}$$

This identity can be used for consistency checking, making sure that two objects in an image are shaded in consistent lighting. This enables detection of inconsistencies, where one object is spliced into an image from another image with inaccurate lighting. Also note that the single image identity (equation 5.3) is just a special case of equation 7.3, where one of the objects is simply a mirror sphere (so, for instance, $B^1 = L$).

7.2 Two Lighting Environments: Same Object/BRDF

We now consider imaging the same object in two different lighting environments. Let us again denote by superscripts 1 or 2 the two images, so that,

$$B_{lm}^1 = A_l L_{lm}^1 \qquad B_{lm}^2 = A_l L_{lm}^2. \tag{7.4}$$

Again, it is possible to eliminate the BRDF by dividing,

$$\frac{B_{lm}^2}{B_{lm}^1} = \frac{L_{lm}^2}{L_{lm}^1} = L_{lm}^{'}. \tag{7.5}$$

We refer to L'_{lm} as the *lighting transfer function.* Given the appearance of an object in lighting condition 1, multiplication of spherical harmonic coefficients by this function gives the appearance in lighting condition 2. L'_{lm} is *independent* of the reflectance or BRDF of the object. Hence, the lighting transfer function obtained from one object can be applied to a different object observed in lighting condition 1. Moreover, we never need to explicitly compute the material properties of any of the objects, nor recover the individual lighting conditions.

The relighting application does not require explicit knowledge of either lighting condition. However, if we assume the lighting conditions are known (unlike the previous subsection, we need the lighting known here since we cannot exploit radial symmetry to eliminate it), equation 7.5 can be expanded in the form of an identity,

$$B^2_{lm}L^1_{lm} - B^1_{lm}L^2_{lm} = 0. \tag{7.6}$$

This identity can be used for consistency checking, making sure that two photographs of an object in different lighting conditions are consistent, and neither has been tampered.

7.3 Two Materials *And* Two Lighting Conditions

Finally, we consider the most conceptually complex case, where both the lighting and materials vary. This effectively corresponds to two images (in different lighting conditions), each containing two objects of different materials. We will now use two superscripts, the first for the lighting and the second for the material.

	Lighting 1	Lighting 2
BRDF 1	$B^{1,1}_{lm} = A^1_l L^1_{lm}$	$B^{2,1}_{lm} = A^1_l L^2_{lm}$
BRDF 2	$B^{1,2}_{lm} = A^2_l L^1_{lm}$	$B^{2,2}_{lm} = A^2_l L^2_{lm}$

Simply by multiplying out and substituting the relations above, we can verify the basic identity discussed in the introduction to this thesis,

$$B^{1,1}_{lm}B^{2,2}_{lm} = B^{1,2}_{lm}B^{2,1}_{lm} = A^1_l A^2_l L^1_{lm}L^2_{lm}, \tag{7.7}$$

or for the purposes of consistency checking,

$$\boxed{B^{1,1}_{lm}B^{2,2}_{lm} - B^{1,2}_{lm}B^{2,1}_{lm} = 0.} \tag{7.8}$$

An interesting feature of this identity is that we have completely eliminated all lighting and BRDF information. Consistency can be checked based simply on the final images, without estimating any illuminations or reflectances. Note that if the second object is a mirror sphere, this case reduces to the two lightings, same BRDF case in equation 7.6.

Equation 7.7 also leads to a simple framework for estimation. The conceptual setup is that we can estimate the appearance of the fourth lighting/BRDF image (without loss of generality, say this is $B_{lm}^{2,2}$), given the other three, *without explicitly computing any illumination or reflectances.* Clearly, this is useful to insert the second object into a photograph where it wasn't present originally, assuming we've seen both objects together under another lighting condition. From equation 7.7, we have

$$\begin{aligned} B_{lm}^{2,2} &= \frac{B_{lm}^{1,2} B_{lm}^{2,1}}{B_{lm}^{1,1}} && (7.9) \\ &= B_{lm}^{1,2} \left(\frac{B_{lm}^{2,1}}{B_{lm}^{1,1}}\right) = B_{lm}^{1,2} L_{lm}^{'} && (7.10) \\ &= B_{lm}^{2,1} \left(\frac{B_{lm}^{1,2}}{B_{lm}^{1,1}}\right) = B_{lm}^{2,1} \gamma_l. && (7.11) \end{aligned}$$

This makes it clear that we can visualize the process of creating $B_{lm}^{2,2}$ in two different ways. Figure 7.1 further illustrates the two approaches. One way (a) is to start with *another* object in the *same* lighting condition, i.e. $B_{lm}^{2,1}$ and apply the BRDF transfer function γ_l. The BRDF transfer function is found from the image of both objects in lighting condition 2. Alternatively (b), we start with the *same* object in another lighting condition $B_{lm}^{1,2}$ and apply the lighting transfer function $L_{lm}^{'}$ obtained from *another* object. In practice, we prefer using the BRDF transfer function (equation 7.11), since γ_l is more robust to noise. The image (e), obtained using lighting transfer function $L_{lm}^{'}$ has artifacts, whereas the one (c), obtained by using BRDF transfer function γ_l is consistent with actual image (d) due to robustness of γ_l to noise. However, the equations above make clear that both interpretations are equivalent, following naturally from equation 7.7.

The idea of estimating the fourth light/BRDF image, given the other three, has some conceptual similarity to learning image analogies [HJO+01]. However, we are considering a convolution of lighting and BRDF, while image analogies try to synthesize images by

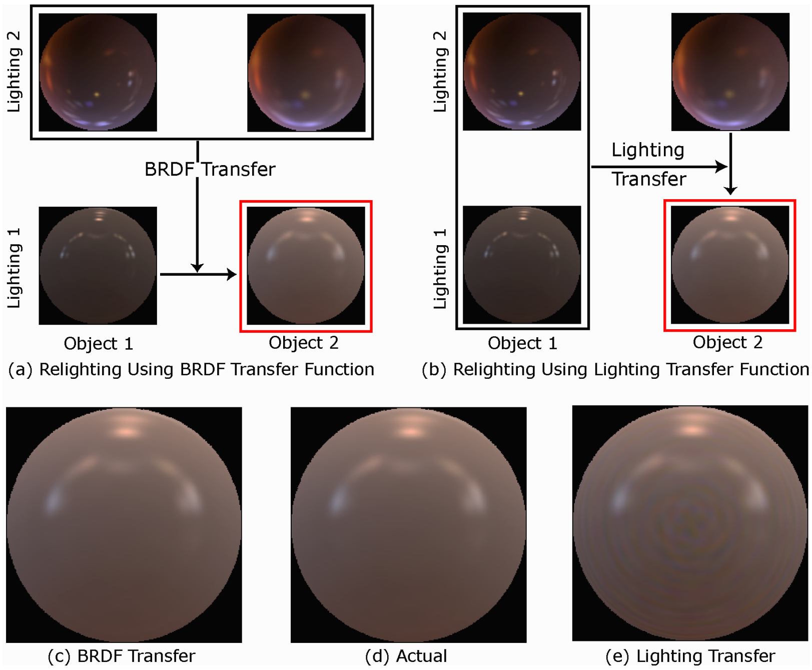

Figure 7.1: **Top Row:** Shows two different approaches for image relighting. We can either use BRDF Transfer function (a) or Lighting Transfer function (b). All the spheres are synthetic, with Lighting 1 being St. Peters environment map and Lighting 2 Grace Cathedral. **Bottom Row:** Comparison of spheres generated using two approaches with actual sphere. Sphere (e) generated using Lighting Transfer has artifacts (note the ringing) whereas the sphere (c) generated using BRDF Transfer matches closely with the acutal sphere (d).

rearranging input pixels, irrespective of the physics, and cannot achieve the desired result in general. Since *none* of the lightings or BRDFs are known, it would also be very difficult to render $B_{lm}^{2,2}$ with alternative physics-based inverse rendering methods.

Chapter 8

Implications and Discussion

We now briefly discuss some of the broader implications of our theory. First, we extend the two BRDF/two lighting case to multiple lighting conditions and BRDFs. Then, we discuss spatial domain setups and identities analogous to our frequency domain analysis. Finally, we show how many previous spatial domain algorithms and invariants can be considered special cases, extensions or variants of this general class of identities.

8.1 Multiple lighting conditions and BRDFs

Let us consider r lighting conditions and s BRDFs, instead of assuming $r = s = 2$, with superscripts $i \leq r$ and $j \leq s$, so that

$$B_{lm}^{i,j} = A_l^j L_{lm}^i \qquad \Longrightarrow \qquad \mathbf{B}_{lm} = \mathbf{L}_{lm} \mathbf{A}_l^T, \tag{8.1}$$

where in the last part, for a given spherical harmonic index (l, m), we regard $\mathbf{B}_{lm}$ as an $r \times s$ matrix obtained by multiplying column vectors $\mathbf{L}_{lm}$ $(r \times 1)$, corresponding to the lighting conditions, and the transpose of $\mathbf{A}_l$ $(s \times 1)$, corresponding to the BRDFs.

Equation 8.1 makes it clear that there is a *rank 1 constraint* on the $r \times s$ matrix $\mathbf{B}_{lm}$. Section 7.3 has considered the special case $r = s = 2$, corresponding to a 2×2 matrix, where the rank 1 constraint leads to a single basic identity (equation 7.8). In fact, equation 7.8 simply states that the determinant of the singular 2×2 matrix $\mathbf{B}_{lm}$ is zero.

8.2 Spatial Domain Analog

Equation 8.1 expresses the image of a homogeneous glossy material in the *frequency domain* as a *product* of lighting and BRDF. Analogously, a difficult to analyze frequency domain convolution corresponds to a simple spatial domain product. For example, the image of a textured Lambertian surface in the *spatial domain* is a *product* of albedo ρ_k and irradiance E_k, where k denotes the pixel.

$$B_k^{i,j} = \rho_k^j E_k^i \qquad \Longrightarrow \qquad \mathbf{B}_k = \mathbf{E}_k \rho_k^T. \tag{8.2}$$

Equation 8.2 has the same product form as the basic convolution equation ($B_{lm} = A_l L_{lm}$). Hence an identity similar to equation 7.8 holds in the angular domain for textured Lambertian objects.

$$B^{1,1}_{\text{diffuse}}(\theta,\phi) B^{2,2}_{\text{diffuse}}(\theta,\phi) = B^{1,2}_{\text{diffuse}}(\theta,\phi) B^{2,1}_{\text{diffuse}}(\theta,\phi) \tag{8.3}$$

The BRDF transfer function $\gamma(\theta,\phi)$ is just the ratio of diffuse albedos and is constant for homegeneous objects.

These identities enable spatial domain techniques for re-rendering the diffuse component (which in our case has constant albedo since the material is homogeneous), while still using the frequency domain for the specular component. In order to separate the diffuse and specular components from the images, we observe that in a parameterization by surface normals, B_{lm} will have essentially all of its diffuse energy for $l \leq 2$, while the specular energy falls away much more slowly [RH02], and therefore mostly resides in $l > 2$. So we assume that

$$B_{\text{diffuse}}(\theta,\phi) \approx \sum_{l=0}^{2} \sum_{m=-l}^{l} B_{lm} Y_{lm}(\theta,\phi) \tag{8.4}$$

But a single image gives information only for a hemisphere of surface normals, so we cannot directly calculate B_{lm} for normal parameterization. Spherical harmonics do not form a linearly independent basis for the hemisphere. We pose the diffuse computation as a fitting problem where we want to find B_{lm}, $l \leq 2$ that best fits the hemisphere. We solve a system of equations $AX = B$ corresponding to equation 8.4, where A is a $N \times 9$ matrix of Y_{lm} computed at sample points on hemisphere, X is a 9×1 matrix of 9 B_{lm} and B is a $N \times 1$ matrix of irradiance at sample points. The specular component can then be handled as discussed in the previous section and the diffuse component can be computed using equation 8.3. The diffuse computation is more stable in the angular domain than in the spherical harmonics domain. This method is used in all our rendering examples. As expected, our practical results work less well for the extremes when the specular intensity is very small relative to the diffuse component (in the limit, a purely Lambertian surface) or vice versa (a purely specular object).

8.3 Analogies with Previous Spatial Domain Results

While the exact form of, and rank 1 constraint on, equation 8.2 is not common in previous work, many earlier spatial domain invariants and algorithms can be seen as using special cases and extensions thereof. We briefly discuss some prominent results in our framework, also describing our analogous frequency domain results. In this way, we provide a unified view of many spatial and frequency domain identities, that we believe confers significant insight.

Reflectance ratios [NB96] are widely used for recognition. The main observation is that at adjacent pixels, the irradiance is essentially the same, so that the ratio of image intensities corresponds to the ratio of albedos. Using superscripts for the different pixels as usual (we do not need multiple super- or any subscripts in this case), we have $B^2/B^1 = \rho^2/\rho^1$. The analogous frequency domain result is equation 7.2, corresponding to the two BRDFs, same lighting case. In both cases, by dividing the image intensities (spherical harmonic coefficients), we obtain a result *independent of the illumination.*

Similarly, a simple version of the recent BRDF-invariant stereo work of Davis et al. [DYW05] can be seen as the two lighting, same BRDF case. For fixed view and point source lighting, a variant of equation 8.2 still holds, where we interpret ρ_k^j as the (spatially varying) BRDF for pixel k and fixed view, and E_k^i as the (spatially varying) light intensity at pixel k. If the light intensity changes (for the same pixel/BRDF), we have $B^2/B^1 = E^2/E^1$. The frequency domain analog is equation 7.5. In both cases, we have *eliminated the BRDF* by dividing image intensities or spherical harmonic coefficients.

Narasimhan et al. [NRN03] also assume point source lighting to derive photometric invariants in the spatial domain—note that our frequency domain framework, by contrast, easily handles general complex lighting. However, we would like to point that we assume curved homegeneous objects of known geometry. Moreover while our identities operate globally needing the full range of reflected directions, spatial domain invariants involve mostly local pixel-based operations. Narasimhan et al. [NRN03] consider a variant of equation 8.2 with a summation of multiple terms (such as diffuse plus specular). For each term, ρ encodes a material property such as the diffuse albedo, while E encodes the illumination intensity and geometric attributes (such as a cosine term for diffuse or a cosine lobe for specular). Their work can be seen as effectively deriving a rank constraint on $\mathbf{B}$, corresponding to the number of terms summed. For diffuse objects, this is a rank 1 constraint, analogous to that in the frequency domain for equation 8.1. For diffuse plus specular, this is a rank 2 constraint. They then effectively use the rank constraint to form appropriate determinants that eliminate either material or geometry/lighting attributes, as in our frequency domain work. Jin et al. [JSY03] employ a similar rank 2 constraint for multi-view stereo with both Lambertian and specular reflectance.

Finally, we note that while there are many analogies between previous spatial domain identities and those we derive in the spherical/angular frequency domain, *some of our frequency domain results have no simple spatial domain analog.* For example, the concept of angular radial symmetry does not transfer to the spatial domain, and there is no known spatial analog of the identities in equations 5.3, 5.4, 6.3, 6.5, and 7.3.

Chapter 9

Experimental Validation and Results

We now present some experiments to validate the theory, and show potential applications. We start with diffuse plus specular spheres in figure 9.1, since they correspond most closely with our theory. We then describe results with a complex cat geometry (figures 1.1, 9.2 and 9.3). All of these results show that the theory can be applied in practice with real data, where objects are not perfectly homogeneous, there is noise in measurement and calibration, and specular reflectance is not perfectly radially symmetric.

Experimental Setup

We ordered spheres from http://www.mcmaster.com. The cat model was obtained at a local craft sale. All objects were painted to have various specular finishes and diffuse undercoats. While homogeneous overall, small geometric and photometric imperfections on the objects were visible at pixel scale and contributed "reflection noise" to the input images. To control lighting, we projected patterns onto two walls in the corner of a room. We placed a Canon EOS 10D camera in the corner and photographed the objects at a distance of 2-3m from the corner (see top left of figure 9.1). This setup has the advantage of more detailed frontal reflections, which are less compressed than those at grazing angles. However, frontal lighting also gives us little information at grazing angles, where the BRDF might violate the assumption of radial symmetry due to Fresnel effects; we hope to address

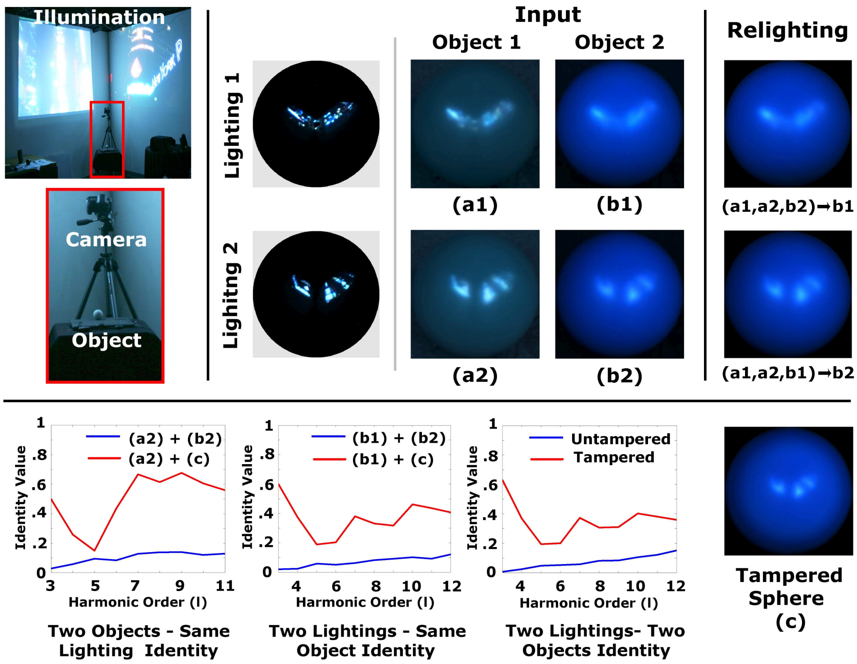

Figure 9.1: **Top Left:** Experimental setup. **Top Middle:** Two lightings (shown only for reference) and images of two glossy (diffuse plus specular) spheres in that lighting. **Top Right:** We can accurately render (b1), given (a1,a2,b2), and render (b2), given (a1,a2,b1). **Bottom:** We tamper (b2) to generate (c) by squashing the specular highlights slightly in photoshop. While plausible to the naked eye, all three identities in chapter 7 clearly indicate the tampering (red graphs).

this limitation in future experiments. To measure the lighting, we photographed a mirror sphere. To measure BRDFs (only for deconvolution), we imaged a sphere under a point source close to the camera, determining A_l by simply reading off the profile of the highlight, and K_d by fitting to the diffuse intensity. For all experiments, we assembled high-dynamic range images.

Glossy Spheres

Figure 9.1 shows the two lighting, two materials case. The top right shows a relighting application. We assume (b1) is unknown, and we want to synthesize it from the other 3 lighting/BRDF images (a1,a2,b2). We also do the same for rendering (b2) assuming we know (a1,a2,b1). The results are visually quite accurate, and in fact reduce much of the

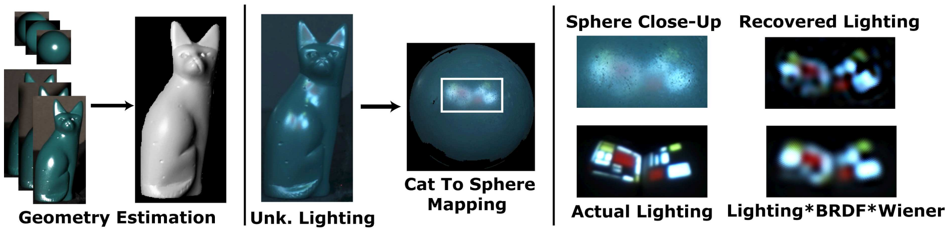

Figure 9.2: Deconvolution on a real cat image. **Left:** Geometry estimation, using example-based photometric stereo (we take a number of images with the cat and example sphere; the sphere is also used to find the BRDF). **Middle:** Input image under unknown lighting, and mapping to a sphere using the surface normals. **Right:** Closeups, showing the original sphere map, and our deconvolved lighting estimate on top. This considerably sharpens the original, while removing noise, and resembles the BRDF*Wiener filter applied to the actual lighting (bottom row).

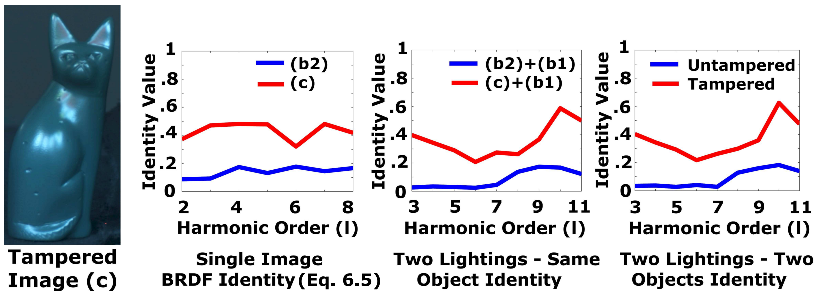

Figure 9.3: Image consistency checking for cat (labels are consistent with figure 1.1). The tampered image (c) is obtained by splicing the top half (b1) under lighting 1 and the bottom half (b2) under lighting 2. Image (c) looks quite plausible, but the splicing is clearly detected by our identities.

noise in the input. Quantitatively, the L_1 norm of the errors for (b1) and (b2) are 9.5% and 6.5% respectively. In the bottom row, we tamper (b2) by using image processing to squash the highlight slightly. With the naked eye, it is difficult to detect that image (c) is not consistent with lighting 2 or the other spheres. However, all three identities discussed in the previous chapter correctly detect the tampering.

Complex Geometry

For complex (mostly convex) known geometry, we can map object points to points on the sphere with the same surface normal, and then operate on the resulting spherical image. Deconvolution is shown in figure 9.2. We used a sphere painted with the same material as the cat to aquire both the cat geometry, using example-based photometric stereo [HS05] for the normals, and the BRDF (needed only for deconvolution). Errors (unrelated to our algorithm) in the estimated geometry lead to some noise in the mapping to the sphere. Our deconvolution method for lighting estimation substantially sharpens the reflections, while removing much of the input noise. Moreover, our results are consistent with taking the actual lighting and convolving it with the product of the BRDF and Wiener spherical harmonic filters.

The cat can also be used directly as an object for relighting/rendering and consistency checking. An example of rendering is shown in figure 1.1. The L_1 norm of the error is somewhat higher than in figure 9.1, at 12%, primarily because this is a much more challenging example. We are using the BRDF transfer function from a much lower-frequency material to a higher-frequency one—the blue sphere has a much broader specular lobe than the green cat. Moreover, inaccuracies in the normal estimation (not part of our algorithm) lead to some visible contouring in the results. Nevertheless, we see that the results are visually plausible. Figure 9.3 illustrates photomontage image tampering, in which the top half under lighting 1 (b1 in figure 1.1) is spliced with the bottom half under lighting 2 (b2 in figure 1.1). While the image (c) looks plausible in itself, the identities for both single and multiple images clearly detect the tampering.

Chapter 10

Conclusions and Future Work

In this thesis, we have introduced a new theoretical framework for using spherical convolution and deconvolution in inverse rendering, BRDF/lighting transfer and image consistency checking. The main contribution is the set of new frequency space formulae, which represent fundamental identities following from the convolution theorem. These identities often eliminate the lighting and/or BRDF, enabling a new class of inverse rendering algorithms that can relight or change materials by using BRDF/lighting transfer functions, without explicit illumination or BRDF estimation. In the future, similar ideas may be applied to other problems, such as BRDF-invariant stereo and photometric stereo, or lighting-insensitive recognition. The theoretical framework also makes a contribution to the relatively new area of image consistency checking, describing a suite of frequency domain identities to detect tampering and other undesirable image processing operations. We have also presented a new unified view of spatial and frequency domain identities and rank constraints, that can give insight for developing future algorithms in either, or even a combination of both domains.

In the future, from a theoretical perspective, we want to develop a framework for operating on local subsets of the entire image, corresponding to small portions of the full sphere of directions. From a practical perspective, we want to better understand the sensitivity of our identities—initial tests indicate they are fairly robust, but more work needs to be done. We wish to apply our algorithms in more complex cases like faces where the geometry is not known accurately, and where objects may not be perfectly convex. We would also like to handle textured objects by automatic diffuse/specular separation methods [MZB06]. We believe that the theory may also lead to the construction of better light probes where we can replace the mirror sphere by a sphere of general material and hence bypass the serious issues like dynamic range associated with current light probes.

In summary, we see this thesis as introducing the basic theory, that can lead to much future theoretical and practical work in inverse rendering and image consistency checking.

Appendix A

Deconvolution - Angular Domain Analysis

$$f(x,m,s) = \int_{-m}^{m} e^{\frac{u^2}{2s}} e^{2\pi i x u} du \tag{A.1}$$

where m is the cutoff frequency. Putting $u = \sqrt{2s}v$

$$f(x,m,s) = \sqrt{2s} \int_{\frac{-m}{\sqrt{2s}}}^{\frac{m}{\sqrt{2s}}} e^{v^2} e^{2\sqrt{2s}\pi i v x} dv \tag{A.2}$$

$$\begin{aligned} f(x,m,s) &= \sqrt{2s} g(\sqrt{2s}x, \frac{m}{\sqrt{2s}}) & \text{(A.3)} \\ g(x,k) &= \int_{-k}^{k} e^{t^2} e^{2\pi i t x} dt \\ &= e^{\pi^2 x^2} \int_{-k}^{k} e^{(t+i\pi x)^2} dt \\ &= e^{\pi^2 x^2} \int_{-k+i\pi x}^{k+i\pi x} e^{z^2} dz & \text{(A.4)} \end{aligned}$$

Since function e^{z^2} is analytic, its integration along closed rectangular path $(-k + i\pi x, k + i\pi x, k, -k, -k + i\pi x)$ is 0, which gives

$$g(x,k) = e^{\pi^2 x^2} [\int_{-k}^{k} e^{t^2} dt + p(x,k)] \tag{A.5}$$

where

$$\begin{aligned} p(x,k) &= \int_{k}^{k+i\pi x} e^{z^2} dz - \int_{-k}^{-k+i\pi x} e^{z^2} dz \\ &= i\pi \int_0^x e^{(k+i\pi t)^2} dt - i\pi \int_0^x e^{(-k+i\pi t)^2} dt \\ &= i\pi e^{k^2} \int_0^x e^{-\pi^2 t^2} [e^{2\pi ikt} - e^{-2\pi ikt}] dt \\ &= -2\pi e^{k^2} \int_0^x e^{-\pi^2 t^2} sin(2\pi kt) dt \end{aligned} \tag{A.6}$$

Hence

$$\begin{aligned} g(x,k) &= e^{\pi^2 x^2} [\int_{-k}^{k} e^{t^2} dt - 2\pi e^{k^2} \int_0^x e^{-\pi^2 t^2} sin(2\pi kt) dt] \\ &= e^{\pi^2 x^2} [(\int_{-k}^{k} e^{t^2} dt - 2\pi e^{k^2} \int_0^\infty e^{-\pi^2 t^2} sin(2\pi kt) dt) + 2\pi e^{k^2} \int_x^\infty e^{-\pi^2 t^2} sin(2\pi kt) dt] \\ &= 2\pi e^{k^2} [e^{\pi^2 x^2} (\frac{e^{-k^2}}{2\pi} \int_{-k}^{k} e^{t^2} dt - \int_0^\infty e^{-\pi^2 t^2} sin(2\pi kt) dt) + \int_x^\infty e^{\pi^2 (x^2 - t^2)} sin(2\pi kt) dt] \\ &= 2\pi e^{k^2} [e^{\pi^2 x^2} q(k) + h(x,k)] \end{aligned} \tag{A.7}$$

where

$$q(k) = \frac{e^{-k^2}}{2\pi} \int_{-k}^{k} e^{t^2} dt - \int_0^\infty e^{-\pi^2 t^2} sin(2\pi kt) dt \tag{A.8}$$

$$h(x,k) = \int_x^\infty e^{\pi^2 (x^2 - t^2)} sin(2\pi kt) dt \tag{A.9}$$

Using Mathematica, we get

$$\int_{-k}^{k} e^{t^2} dt = \sqrt{\pi} Erfi(k) \tag{A.10}$$

$$\int_0^\infty e^{-\pi^2 t^2} sin(2\pi kt) dt = \frac{e^{-k^2} Erfi(k)}{2\sqrt{\pi}} \tag{A.11}$$

where $Erfi(z)$ is the imaginary part of $\frac{2}{\sqrt{\pi}} \int_0^{iz} e^{-t^2} dt$. Hence $q(k) = 0$.

$$\begin{aligned} g(x,k) &= 2\pi e^{k^2} [e^{\pi^2 x^2} q(k) + h(x,k)] \\ &= 2\pi e^{k^2} h(x,k) \end{aligned} \tag{A.12}$$

$$h(x,k) = \int_x^\infty e^{\pi^2 (x^2 - t^2)} sin(2\pi kt) dt \tag{A.13}$$

Substituting $u = kt$

$$\begin{aligned} h(x,k) &= \int_x^\infty e^{\pi^2(x^2-t^2)} sin(2\pi kt)dt \\ &= \frac{1}{k}\int_{kx}^\infty e^{\frac{\pi^2}{k^2}(k^2x^2-u^2)} sin(2\pi u)du \\ &= \frac{1}{k}n(kx, \frac{\pi}{k}) \end{aligned} \tag{A.14}$$

where

$$n(\alpha, \beta) = \int_\alpha^\infty e^{\beta^2(\alpha^2-u^2)} sin(2\pi u)du \tag{A.15}$$

Appendix B

Analysis of D_{nm}

First, let $E(\alpha, \beta)$ be the diffuse irradiance parameterized in the usual way by the surface normal,

$$E(\alpha, \beta) \approx \sum_{n=0}^{\infty} \sum_{u=-n}^{n} A_n^{Lamb} L_{nu} Y_{nu}(\alpha, \beta), \tag{B.1}$$

where as usual, a very good approximation can be obtained with $n \leq 2$ for Lambertian reflectance. Let $D(\alpha, \beta)$ represent the irradiance parameterized by the reflection vector. Assuming that the coordinate system is aligned so the viewer is on the positive z axis, a normal (α, β) corresponds to a reflection vector $(2\alpha, \beta)$. Conversely, a reflected direction (α, β) corresponds to a normal $(\alpha/2, \beta)$,

$$D(\alpha, \beta) \quad = \quad E(\frac{\alpha}{2}, \beta). \tag{B.2}$$

Consider the spherical harmonic coefficients D_{lm} of $D(\alpha, \beta)$, (and with Y_{lm}^* being the complex conjugate of the spherical harmonic Y_{lm}),

$$\begin{aligned} D_{lm} &= \int_{S^2} D(\alpha, \beta) Y_{lm}^*(\alpha, \beta) d\Omega & \text{(B.3)} \\ &= \int_{S^2} E(\frac{\alpha}{2}, \beta) Y_{lm}^*(\alpha, \beta) d\Omega. & \text{(B.4)} \end{aligned}$$

We now substitute for $E(\alpha/2, \beta)$ in terms of spherical harmonic coefficients, and move the summations out of the integral,

$$D_{lm} = \sum_{n=0}^{\infty} \sum_{u=-n}^{n} \int_{S^2} A_n^{Lamb} L_{nu} Y_{nu}(\frac{\alpha}{2}, \beta) Y_{lm}^*(\alpha, \beta) d\Omega \tag{B.5}$$

$$= \sum_{n=0}^{\infty} \int_{S^2} A_n^{Lamb} L_{nm} Y_{nm}(\frac{\alpha}{2}, \beta) Y_{lm}^*(\alpha, \beta) d\Omega, \tag{B.6}$$

where in the last line, we have used orthogonality of spherical harmonics for the integral over β, to require that $u = m$. Continuing,

$$D_{lm} = \sum_{n=0}^{\infty} A_n^{Lamb} L_{nm} \int_{S^2} Y_{nm}(\frac{\alpha}{2}, \beta) Y_{lm}^*(\alpha, \beta) d\Omega \tag{B.7}$$

$$= \sum_{n=0}^{\infty} A_n^{Lamb} L_{nm} T_{lmn}, \tag{B.8}$$

where

$$T_{lmn} = \int_{S^2} Y_{nm}(\frac{\alpha}{2}, \beta) Y_{lm}^*(\alpha, \beta) d\Omega. \tag{B.9}$$

Since n ranges from 0 to 2, m varies from -2 to 2, and we can neglect terms with $\mid m \mid > 2$ or $\mid n \mid > 2$,

$$D_{lm} \approx \sum_{n=0}^{2} A_n^{Lamb} L_{nm} T_{lmn}. \tag{B.10}$$

So we need to consider T_{lmn} for $n = 0, 1, 2$ and $\mid m \mid \leq n$, which is a total of only 9 (m, n) pairs. Note that this means we can safely neglect the effects of the diffuse component for $\mid m \mid > 2$, in calculating identities. Figure 6.2(a)-(b) shows plots of D_{lm} for small and large values of l respectively, for a particular complex natural lighting environment.

The coefficients T_{lmn} are simple numerical constants, which can be determined analytically in some cases. In general, the integrals can be difficult to do analytically, and we determine the coefficients by numerical integration, directly from the definition in equation B.9. This is easy since we know the analytic forms of the spherical harmonics.

We have also analyzed the numerical values of the coefficients T_{lmn}. For $l = 0$, only $T_{000} = 1$, and other terms are zero (since $\mid m \mid \leq n$ and $\mid m \mid \leq l$). Also, for $l \geq 2$, we find that $T_{l00} = T_{l02} = T_{l-12} = T_{l12} = 0$. Also T_{l01} falls off as $n^{-2.5}$, $T_{l11} = T_{l-11}$ as $l^{-1.5}$ and

$T_{l22} = T_{l-22}$ also varies as $l^{-1.5}$. Figure 6.2(c) shows the fall off of T_{lmn} with increasing values of l.

Because many of the T_{lmn} terms are 0, we can substantially simplify the value of D_{lm}. In particular, if $m = 0$, then we must have $n = 1$ for $l \geq 2$, so that

$$D_{(l\geq 2)0} \quad = \quad A_1^{Lamb} L_{10} T_{l01}. \tag{B.11}$$

Similarly, if $\mid m \mid = 1, 2$ and $l \geq 2$, the only nonzero terms have $n = \mid m \mid$, and we can write

$$D_{(l\geq 2)m} = A_{|m|}^{Lamb} L_{|m|m} T_{lm|m|}. \tag{B.12}$$

References

[BJ01] R. Basri and D. Jacobs. Photometric stereo with general, unknown lighting. In *CVPR 01*, pages II–374–II–381, 2001.

[BJ03] R. Basri and D. Jacobs. Lambertian reflectance and linear subspaces. *PAMI*, 25(2):218–233, 2003.

[DYW05] J. Davis, R. Yang, and L. Wang. BRDF invariant stereo using light transport constancy. In *ICCV 05*, 2005.

[GW03] R. Gonzalez and R. Woods. *Digital Image Processing, Second Edition.* Pearson Education, 2003.

[HJO+01] A. Hertzmann, C. Jacobs, N. Oliver, B. Curless, and D. Salesin. Image analogies. In *SIGGRAPH 01*, pages 327–340, 2001.

[HS05] A. Hertzmann and S. Seitz. Example-based photometric stereo: Shape reconstruction with general, varying BRDFs. *PAMI*, 27(8):1254–1264, 2005.

[JF05] M. Johnson and H. Farid. Exposing digital forgeries by detecting inconsistencies in lighting. In *ACM Multimedia and Security Workshop*, 2005.

[JSY03] H. Jin, S. Soatto, and A. Yezzi. Multi-view stereo beyond lambert. In *CVPR 03*, pages 171–178, 2003.

[LWTS05] Z. Lin, R. Wang, X. Tang, and H. Shum. Detecting doctored images using camera response normality and consistency. In *CVPR 05*, 2005.

[MG97] S. Marschner and D. Greenberg. Inverse lighting for photography. In *Color Imaging Conf.*, pages 262–265, 1997.

[MRC06] Dhruv Mahajan, Ravi Ramamoorthi, and Brian Curless. A theory of spherical harmonic identities for brdf/lighting transfer and image consistency. In *ECCV 06*, 2006.

[MWLT00] S.R. Marschner, S.H. Westin, E.P.F. Lafortune, and K.E. Torrance. Image-Based BRDF measurement. *Applied Optics*, 39(16):2592–2600, 2000.

[MZB06] Satya Mallick, Todd Zickler, and Peter Belhumeur. Specularity removal in images and videos: A pde approach. In *ECCV 06*, 2006.

[NB96] S. Nayar and R. Bolle. Reflectance based object recognition. *IJCV*, 17(3):219–240, 1996.

[NCS04] T. Ng, S. Chang, and Q. Sun. Blind detection of photomontage using higher order statistics. In *IEEE International Symposium on Circuits and Systems*, 2004.

[NRN03] S. Narasimhan, V. Ramesh, and S. Nayar. A class of photometric invariants: Separating material from shape and illumination. In *ICCV 03*, pages 1387–1394, 2003.

[RH01a] R. Ramamoorthi and P. Hanrahan. An efficient representation for irradiance environment maps. In *SIGGRAPH 01*, pages 497–500, 2001.

[RH01b] R. Ramamoorthi and P. Hanrahan. A signal-processing framework for inverse rendering. In *SIGGRAPH 01*, pages 117–128, 2001.

[RH02] R. Ramamoorthi and P. Hanrahan. Frequency space environment map rendering. *ACM Transactions on Graphics (SIGGRAPH 2002)*, 21(3):517–526, 2002.

[Rus98] S. Rusinkiewicz. A new change of variables for efficient brdf representation. In *Eurographics Rendering Workshop*, 1998.

[SFB03] D. Simakov, D. Frolova, and R. Basri. Dense shape reconstruction of a moving object under arbitrary, unknown lighting. In *ICCV 03*, pages 1202–1209, 2003.

[SKS02] P. Sloan, J. Kautz, and J. Snyder. Precomputed radiance transfer for real-time rendering in dynamic, low-frequency lighting environments. *ACM Transactions on Graphics (SIGGRAPH 2002)*, 21(3):527–536, 2002.

[SSI99] I. Sato, Y. Sato, and K. Ikeuchi. Illumination distribution from brightness in shadows: adaptive estimation of illumination distribution with unknown reflectance properties in shadow regions. In *ICCV 99*, pages 875 – 882, 1999.

[Wie42] N. Wiener. Extrapolation, interpolation and smoothing of stationary time series. In *the MIT Press*, 1942.